High-Efficiency On-Chip Frequency Conversion in the Telecom Band

Yun Zhao^{1,*}, Bok Young Kim², Xingchen Ji¹, Yoshitomo Okawachi², Michal Lipson^{1,2}, and Alexander L. Gaeta^{1,2}

¹Department of Electrical Engineering, Columbia University, New York, NY 10027, USA
²Department of Applied Physics and Applied Mathematics, Columbia University, New York, NY 10027, USA
Author e-mail address: yz3019@columbia.edu

Abstract: Using silicon-nitride microresonators with integrated Moiré-Bragg gratings to suppress parasitic nonlinear processes, we demonstrate on-chip frequency conversion to a single idler tone with a record-high 71% efficiency using Bragg scattering four-wave-mixing. © 2022 The Author(s)

Optical frequency conversion (OFC) is an important tool for both classical and quantum optics applications, including all-optical switching, optical transduction, temporal mode sorting, and temporal magnification. Typically, OFC is performed using $\chi^{(2)}$ materials, which can achieve \leq 50 GHz frequency shifts via the electro-optic (EO) effect or \geq 100 THz frequency shifts via sum/difference frequency generation. For intermediate frequency shifts, including the channel spacings defined by the International Communications Union (ITU), OFC cannot be easily realized with $\chi^{(2)}$ materials. However, through use of $\chi^{(3)}$ processes, such as Bragg scattering four-wave-mixing (BS-FWM), wideband frequency translation spanning from near-DC to several hundreds of THz can be readily performed. Moreover, since $\chi^{(3)}$ nonlinearities are present in all materials, the BS-FWM process can be implemented on all photonic platforms. To date, the highest on-chip BS-FWM efficiency reported is 60%, which is achieved for a 115-THz frequency shift [1]. An air cladded device was used in order to achieve normal group-velocity-dispersion (GVD) for both pumps while maintaining comparable free spectral range (FSR) for the two frequency bands, which requires two largely separated zero-GVD points between the pumps. For frequency shifts below 50 THz, demonstrated efficiencies range from 10% to 25% due to weak nonlinearities and difficulties in suppressing unwanted four-wave-mixing (FWM) processes [1-5]. Several approaches have been proposed for suppressing these parasitic processes [6-10], however efficiencies >1% have not been shown in corresponding demonstrations [6, 8, 9], due to further reduced nonlinearities or difficulties in device control of these systems.

Here, we demonstrate OFC within the telecommunication band with 71% efficiency using BS-FWM in a siliconnitride microresonator, which represents the highest efficiency in $\chi^{(3)}$ -chip based platforms, and nearly a 3-fold improvement to previous telecom-domain OFCs. This performance is achieved by implementing Moiré-Bragg gratings on the waveguide structure to create narrow-band mode coupling between the clockwise (CW) and counterclockwise (CCW) modes, which serve to suppress the resonances related to parasitic FWM processes.

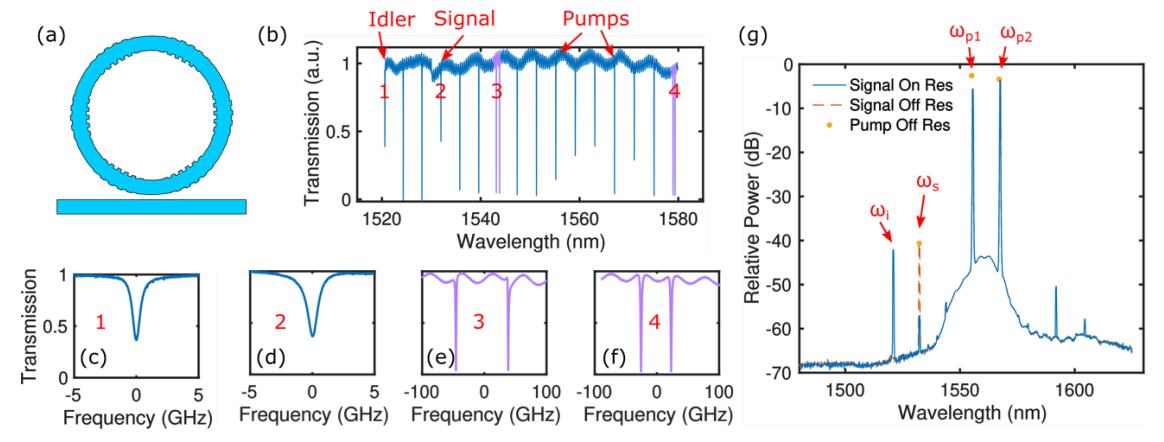


Fig. 1. (a) Illustration of the microring resonator with modulated Bragg grating. Structure is not up to scale. (b) Transmission scan of the fabricated device. The resonances highlighted in purple correspond to 2 of the 3 mode interaction regions. (c)-(f) Zoom in scan of the non-interacting idler and signal modes (1 and 2) and the mode interactions (3 and 4) and. (g) Recorded spectrum with high conversion efficiency.

It has been shown that periodic structures along the microring with an angular periodicity of π/n creates coupling between the *n*th CW and CCW frequency modes [11]. By adding a grating-size modulation of $1 + A\cos(2m\theta)$ to this

Bragg grating, we can add two additional coupling regions at the $n \pm m$ th modes [Fig. 1 (a)], where A is the modulation strength, and θ is the angle. This is attributed to the Moiré effect and the structure is referred to as Moiré-Bragg grating [12]. We choose the BS-FWM process to satisfy energy conservation $\omega_{p1} + \omega_i = \omega_{p2} + \omega_s$, where $\omega_{p1}, \omega_{p2}, \omega_s$, and ω_i are the frequencies of the red pump, blue pump, signal and idler, respectively, with $\omega_{p1} < \omega_{p2} < \omega_s < \omega_i$. We design the mode interactions to be present at $\omega_s - \Delta \omega$ and $\omega_i + \Delta \omega$ to suppress the unwanted red idler and the cascaded blue idler, respectively, where $\Delta \omega = \omega_i - \omega_s$. Furthermore, we place mode interactions at $\omega_{p1} - \Delta \omega$ and $\omega_{p2} + \Delta \omega$ to suppress stimulated degenerate FWM and avoid the formation of frequency-comb-like structures. In our scheme, we let $\omega_s - \Delta \omega = \omega_{p2} + \Delta \omega = \omega_0$, thus only 3 mode interaction regions are needed. We choose modes n, n-m, and n+m to correspond to ω_0 , $\omega_{p1} - \Delta \omega$, and $\omega_i + \Delta \omega$, respectively [Fig. 1(b)]. We also note that additional modulation frequencies can be added to the Bragg grating which enables the ability to select different pump and signal frequencies.

Due to the presence of self- and cross-phase modulation (SPM and XPM), dual-pumped $\chi^{(3)}$ processes in cavities can experience nonlinear bistability. Moreover, additional phase shifts can be imparted due to cascaded frequency conversion processes. This effect is readily observed in $\chi^{(2)}$ -based frequency conversions but has not been analyzed in $\chi^{(3)}$ processes. Recently, it has been shown that in $\chi^{(2)}$ -cavity-based systems the highest conversion efficiency is always achieved under a nonlinear critical coupling condition [13] which corresponds to the following two equalities: the signal conversion rate being equal to the linear loss rate, and the sum of the signal's linear detuning and nonlinear phase shift being equal to 0, where the nonlinear phase shift must include contributions from the cascaded conversion process. Using similar analysis, we can show that the same condition applies to the BS-FWM process. Importantly, our analysis shows that given sufficient pump power, optimizing pump and signal detuning is sufficient to reach the maximum conversion efficiency. Furthermore, the conventional phase matching condition, that is the zero-GVD point being at the center of the frequencies, is not required, though a strong violation of this condition increases the required pump power. This allows us to tailor the GVD to suppress the broad-band modulation instability process.

In our experiment, we design the microring cross-section to be 730 ×1050 nm, which exhibits normal GVD for wavelengths longer than 1512 nm. This is used to suppress degenerate FWM from individual pumps. The FSR is measured to be 488 GHz in the telecom band. We design the grating's angular period to be $\pi/326$ which corresponds to 1543.5 nm. The modulation on the grating has a period of $\pi/9$ which corresponds to additional mode crossings at 1579.3 nm and 1509.3 nm. The modulation is implemented such that the maximum grating size is 50 nm and the minimum is 0, which corresponds to mode splitting strengths of 84 GHz and 48 GHz at 1543.5 nm and 1579.3 nm, respectively. We design the ring-bus coupling to be in the strongly overcoupled regime to enable a large efficiency upper bound [13]. The signal and idler modes have a loaded O of 1.9×10^5 from which we infer an intrinsic O of 1×10^6 [Fig. 1(c) and (d)]. We use 138 mW, 148 mW, and 21 μW for pump 1, 2, and signal, respectively. Both pumps are kept on the blue sides of their respective resonances while the signal is tuned to maximize the conversion efficiency. As shown in Fig. 1(g), the signal is depleted to a level of 15 dB lower than that of the generated idler. We note that a stronger depletion of the signal can also be achieved in our experiment, but this leads to a lower conversion efficiency since it deviates from the nonlinear-critical-coupling condition. We calibrate the input signal power in the spectral measurement by slightly detuning the signal such that the idler becomes unobservable, which indicates that the net conversion efficiency is 71%. An alternative calibration is performed by tuning the pumps off resonance while keeping the signal at its optimal frequency, which agrees with the first calibration. Critically, only a single idler component is generated in our experiment, which is attributed to the induced mode crossing by the grating.

References

- [1] Q. Li, M. Davanço, and K. Srinivasan, Nat. Photonics 10, 406 (2016).
- [2] I. Agha, M. Davanço, B. Thurston, and K. Srinivasan, Opt. Lett. 37, 2997 (2012).
- [3] K. Saha, Y. Okawachi, O. Kuzucu, M. Menard, M. Lipson, and A. L. Gaeta, in CLEO:2013 OSA Technical Digest (online) (Optical Society of America, 2013), paper QF1D.2.
- [4] Y. Zhao, D. Lombardo, J. Mathews, and I. Agha, APL Photonics 2, 026102 (2017).
- [5] K. Li, H. Sun, and A. C. Foster, Opt. Lett. 42, 1488 (2017).
- [6] B. Bell, C. Xiong, D. Marpaung, C. J. McKinstrie, and B. J. Eggleton, Opt. Lett. 42, 1668 (2017).
- [7] J. B. Christensen, J. G. Koefoed, B. A. Bell, C. J. McKinstrie, and K. Rottwitt, Opt. Express 26, 17145 (2018).
- [8] M. Heuck, J. G. Koefoed, J. B. Christensen, Y. Ding, L. Frandsen, K. Rottwitt, and Leif Oxenløwe, New J. Phys. 21, 033037 (2019).
- [9] C. Lacava, M. A. Ettabib, T. D. Bucio, G. Sharp, A. Z. Khokhar, Y. Jung, M. Sorel, F. Gardes, D. J. Richardson, P. Petropoulos, and F. Parmigiani, J. Lightwave Techol. 37, 1680 (2019).
- [10] J. Liu, Q. Zheng, G. Xia, C. Wu, Z. Zhu, and P. Xu, Opt. Express 29, 36038 (2021).
- [11] X, Lu, S. Rogers, W. C. Jiang, and Q. Lin, Appl. Phys. Lett. 105, 151104 (2014).
- [12] D. C. J. Reid, C. M. Ragdale, I. Bennion, D. J. Robbins, J. Buss, and W. J. Stewart, Electron. Lett. 26, 10 (1990).
- [13] Y. Zhao, J. K. Jang, Y. Okawachi, and A. L. Gaeta, Opt. Lett. **46**, 5393 (2021).